Applied Physics Letters ARTICLE scitation.org/journal/apl

Fast attenuation of high-frequency acoustic waves in bicontinuous nanoporous gold

Cite as: Appl. Phys. Lett. **119**, 063101 (2021); doi: 10.1063/5.0055391
Submitted: 28 April 2021 · Accepted: 29 July 2021 ·
Published Online: 10 August 2021

Q. Zheng,[1,2] Y. Tian,[3] X. Shen,[2] K. Sokolowski-Tinten,[4] R. K. Li,[2] Z. Chen,[2] M. Z. Mo,[2] Z. L. Wang,[5] P. Liu,[1] T. Fujita,[5,6] S. P. Weathersby,[2] J. Yang,[2] X. J. Wang,[2,a)] and M. W. Chen[3,a)]

AFFILIATIONS

[1]School of Materials Science and Engineering, Shanghai Jiao Tong University, 800 Dongchuan Road, Shanghai 200240, China
[2]SLAC National Accelerator Laboratory, 2575 Sand Hill Road, Menlo Park, California 94025, USA
[3]Department of Materials Science and Engineering, Johns Hopkins University, 3400 North Charles Street, Baltimore, Maryland 21218, USA
[4]Faculty of Physics and Centre for Nanointegration Duisburg-Essen, University of Duisburg-Essen, Lotharstrasse 1, 47048 Duisburg, Germany
[5]WPI-Advanced Institute for Materials Research, Tohoku University, Sendai 980-8577, Japan
[6]School of Environmental Science and Engineering, Kochi University of Technology, 185 Miyanokuchi, Tosayamada, Kami City, Kochi 782-8502, Japan

[a)]**Authors to whom correspondence should be addressed:** wangxj@slac.stanford.edu and mwchen@jhu.edu

ABSTRACT

We studied the formation and attenuation of GHz elastic waves in free-standing nanoporous gold films by MeV ultrafast electron diffraction and finite element simulations. By tracing the evolution of the high frequency acoustic waves in time domain, we found that the bicontinuous nanoporous structure in nanoporous gold films results in three-dimensionally acoustic response with low coherence, leading to fast attenuation of the elastic waves in comparison with solid gold films. The morphologically dominated dynamics indicates the nanoporosity plays an important role in the high-frequency acoustic energy relaxation, which shines a light on the applications of dealloyed nanoporous materials in nanodevices and sensors as GHz and THz acoustic filters and dampers.

High-frequency acoustic phonons often play a crucial role in affecting the performances of nanostructured materials and nanodevices, such as the sensitivity in detecting force and mass.[1–3] Picosecond and femtosecond pulsed laser stimulating GHz and THz acoustic waves, detected by ultrafast laser spectroscopy[4–11] and ultrafast x-ray/electron diffraction,[12–15] have become a ubiquitous approach for studying the generation, propagation, and attenuation of the high frequency elastic waves in nanostructured materials and thin films. For metallic materials, the excitation of coherent acoustic phonons occurs via lattice expansion by laser-induced rapid heating.[6] The shapes and sizes of nanoscale objects significantly affect the wavelengths and magnitudes of resulting elastic waves. For objects with a simple geometry, the acoustic waves can be well described by the continuum linear elasticity theory.[16] For example, the acoustic wave frequency of thin films is simply determined by the film thickness, which is often interpreted as the thickness resonance frequency.[17] The high-frequency elastic waves propagating in solids decay over space and time. The material attenuation from inherent structures, such as vacancies, grain boundaries, and dislocations, can be accounted for by an exponential decay factor. Although it has been long known that external structures, such as voids, in bulk solids can significantly affect the attenuation of acoustic waves,[18] the effects of nanostructures, such as nanoscale porosity,[19] on the generation, propagation, and attenuation of high-frequency elastic waves remain largely unknown. In this study, we investigated free-standing nanoporous gold (NPG) films by using a MeV ultrafast electron diffraction (MeV UED) technique to explore how nanoscale porosity affects the acoustic response and energy dissipation in thin metallic films, with the comparison of free-standing solid polycrystalline gold (PCG) films. As we will illustrate below, the bicontinuous porous structure in NPG films gives rise to a three-dimensionally acoustic response with low coherence, leading to rapid attenuation of GHz acoustic waves in NPG films.

Free-standing NPG films with ligament sizes of about 30–50 nm were synthesized by selective leaching of silver from ~100 nm thick $Au_{35}Ag_{65}$ (atomic ratio) films using a 60% (volume ratio)

HNO_3 aqueous solution at room temperature.[20] For reference, we also prepared free-standing PCG solid films with thicknesses of about 30 nm by magnetron dc sputtering on dissolvable single-crystal sodium chloride substrates. Both samples were loaded on empty TEM Cu grids for MeV UED experiments (Fig. 1). Using free-standing samples excludes the effects of environments on energy loss of acoustic waves.[8,12] Time-resolved experiments were conducted using a state-of-the-art MeV UED system at SLAC National Accelerator Laboratory.[21] About 200 μm diameter areas in the NPG and PCG films were uniformly pumped by 400 nm laser pulses with pulse duration of 60 fs in the full width at half-maximum (FWHM). Simultaneously, the lattice response in the central areas with a diameter of ~50 μm was probed by 3.2 MeV electron pulses with a bunch length of 190 fs (rms) in a near normal incident geometry. Since the electron probe is much smaller than the laser-excitation area and orders of magnitude larger than the sample thicknesses, possible interference from other resonant and transient modes can be ignored. After the incidence of femtosecond laser pulses, free electrons in the samples are instantaneously heated up. These hot electrons quickly transfer their energy to lattices by electron–phonon coupling. In particular, the large internal surfaces of NPG promote the electron–phonon interaction for fast energy transfer.[22,23] Considering the transverse sound speed of 1.201 nm/ps and the hot electron diffusion speed of less than 10 nm/ps in gold,[23] it takes about tens of nanoseconds for the probed areas to exchange energy with environment. Since the thickness of both samples is less than the ballistic electron motion range of about 100 nm in gold,[23] the heating is also homogeneous in thickness direction. Therefore, in the time scale of interest (less than 1 ns), the probe areas can be considered homogeneously heated and isolated.

The fs laser induced lattice expansion and resulting acoustic waves are inspected by the shift of diffraction peak positions with MeV UED delay time (Figs. S2 and S3). As the lattice spacings tend to enlarge with the increase in internal energy, the electron diffraction peaks of the face-centered cubic gold lattices shift to smaller diffraction angles. Generally, the electron energy and the lattice energy contribute to the thermal expansion in different levels. So, the total thermal stress changes during the electron–phonon coupling. According to the model proposed by Thomsen *et al.*,[5] we can separate the driving force of thermal expansion in non-magnetic metals into two independent parts from the anharmonicity of lattice vibration and the excited free electrons. If we consider the thermal distributions for both electrons and phonons,[24] the total thermal stress can be described by

$$\sigma(t) = \sigma_e(t) + \sigma_l(t) = -\gamma_e \Delta E_e(t) - \gamma_l \Delta E_l(t), \quad (1)$$

where t is the time delay, and σ_e, γ_e, ΔE_e and σ_l, γ_l, ΔE_l refer to the thermal stress, Grüneisen parameters, and changes in energy density for the electron and lattice subsystems, respectively. Assuming an electron-lattice energy exchange with an exponential time dependence,[12,25] the total thermal stress can be expressed as

$$\sigma(t) = \sigma_\infty[1 - \gamma \exp(-t/\tau)]H(t), \quad (2)$$

where τ is the exponential time constant for electron–phonon coupling, H is the Heaviside function, σ_∞ is the asymptotic rise in total thermal stress, and γ is defined as

$$\gamma \equiv 1 - \gamma_e/\gamma_l. \quad (3)$$

According to the constitutive equation of isotropic linear elastic continuum with infinitesimal strain, namely, Hooke's law, it gives

$$\sigma_\infty = -3K\alpha\Delta T_{l,\infty}, \quad (4)$$

where K is the bulk modulus, α is the coefficient of linear expansion, and $\Delta T_{l,\infty}$ is the asymptotic rise in lattice temperature. Therefore, the thermal stress σ in the samples [Fig. 2(b)], associated with the time constant τ and the asymptotic rise in lattice temperature $\Delta T_{l,\infty}$, can be experimentally determined by the decay of Bragg peak intensity.[22,26] For example, with a pump fluence of 2.61 mJ/cm^2, we obtained $\Delta T_{l,\infty}$ of 156.8 K (σ_∞ of 1213.2 MPa) for NPG and $\Delta T_{l,\infty}$ of 162.4 K (σ_∞ of 1171.7 MPa) for PCG from the decreases of Bragg peak intensity (Fig. S1). According to the relationship between τ and $\Delta T_{l,\infty}$ obtained in our previous publication on electron–phonon coupling in NPG,[22] we have τ of ~4.39 ps for NPG and τ of ~5.95 ps for PCG. The total thermal stress σ increases during the energy transfer from hot electrons to cold lattices due to the smaller γ_e of 1.6 than the γ_l of 2.96 for gold.[27]

The thermal stress drives the materials that expand in allowed dimensions, but only the expansion component perpendicular to the electron probe beam can be directly measured. The detectable overall change in lattice spacings approximately equals to the opposite of the relative change in Bragg peak positions, which can be quantitatively measured by the MeV UED system that has a high reciprocal space resolution in detecting the relative change in Bragg peak positions down to 10^{-4}. For example, $\Delta Q = 0.080$ Å^{-1} relative to $Q_0 \approx 6.8$ Å^{-1} of gold (331)/(420) can be detected. As revealed by the shifts of the Bragg peaks of gold (331)/(420) [Fig. 2(a)], the significant lattice expansions occur in both NPG and PCG samples after the transient excitation. For example, with the pump fluence of 2.61 mJ/cm^2, the observed maximum lattice expansions, characterized by the relative peak position change $\Delta Q/Q_0$, reach ~0.0017 for NPG and ~0.0007 for PCG (Fig. S2). Subsequently, periodic lattice contraction and expansion can be observed in the PCG sample, corresponding to the formation of acoustic waves. The oscillation for PCG has a frequency of 53.8 GHz, which is fairly consistent with the thickness resonance frequency of $2L/v_L$, where L is the film thickness and v_L is the longitudinal sound speed (3.325 nm/ps) in gold.[28] For the solid film, the oscillation can well stand with slight intensity decay during the wave propagation, consistent with a wide range of UED

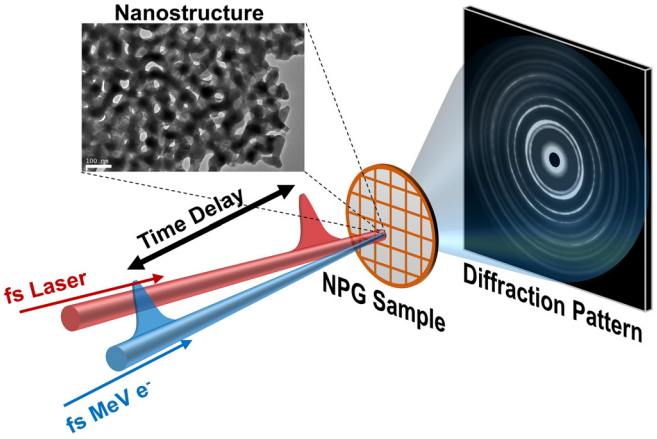

FIG. 1. The schematic of the MeV UED experiments and a TEM image of the NPG sample.

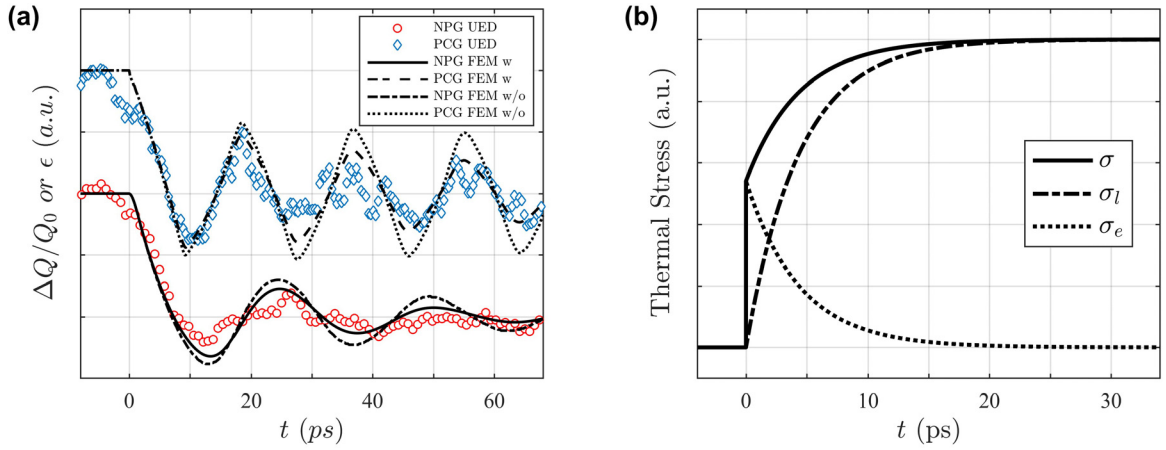

FIG. 2. (a) The changes of Bragg peak position $\Delta Q/Q_0$ of gold (331)/(420) for the NPG and PCG samples. Calculated averaged strain with and without Rayleigh damping factors for both samples are shown. (b) The evolution of the total, electronic, and lattice thermal stress σ, σ_e, σ_l.

observations.[4,12,25] In contrast, the lattice contraction–expansion oscillation, stimulated by the fs laser, quickly decays in the NPG sample, and, in fact, only one well-defined cycle can be observed with a frequency of ∼40.8 GHz. The generation and quick decay of the 40.8 GHz acoustic wave can also be detected from the (220) Bragg peak (Fig. S3). The quick decay of the lattice oscillation in the porous NPG film suggests the fast attenuation of the GHz acoustic waves in the nanoporous material.

To understand acoustic wave formation and attenuation in the nanoporous metal, we conducted finite element method (FEM) calculations. Two linear elastic continuum models of a solid thin gold plate and bicontinuous nanoporous gold with in-plane constraint borders were employed for simulating the dynamic responses of PCG and NPG (Fig. S4). A set of phenomenological Rayleigh damping factors were introduced to imitate the intrinsic inelastic acoustic damping property of gold from the anharmonicity and the scattering of crystal defects, such as vacancies, dislocations, and grain boundaries. We used a mass factor $a_1 = 0.0207\ \mathrm{ps}^{-1}$ and a stiffness factor $a_2 = 0.0190$ ps for the calculations of both PCG and NPG. The damping ratios, $\beta_n/\omega_n = (a_1/\omega_n + a_2 * \omega_n)/2$, of phonons with undamped angular frequencies ω_n between 0.104 and 10.4 THz are less than 10%, where β_n is the damping rate. The calculated averaged strains are fairly consistent with the evolution of (331)/(420) and (220) Bragg peak positions for both NPG and PCG. The oscillation of the calculated averaged strain is approximately with damping rates[29] $\beta_{tot} = 46.9\ \mathrm{ns}^{-1}$ for NPG and $\beta_{tot} = 15.0\ \mathrm{ns}^{-1}$ for PCG (Fig. S9). If Rayleigh damping factors are not considered, the damping rate is $\beta_S = 34.1\ \mathrm{ns}^{-1}$ for NPG, which is significantly larger than $\beta_S = 3.1\ \mathrm{ns}^{-1}$ for PCG. Thus, the nanoporous structure plays an important role in the acoustic wave attenuation. The infinite spatial gradient of step-like strain in theoretical case is limited in FEM calculation, leading to slight dephasing of phonons and thus a small damping rate for PCG even when the Rayleigh damping factors are not considered. The Rayleigh damping factors contribute to the damping rate $\beta_R = \beta_{tot} - \beta_S = 12.8\ \mathrm{ns}^{-1}$ for NPG, comparable with $\beta_R = 11.9\ \mathrm{ns}^{-1}$ for PCG, corresponding to damping ratios of ∼4%.

As an example to illustrate the local dynamics, we compared the time-dependent stress distributions in the NPG and PCG models with the identical pump fluence of 2.61 mJ/cm^2. At the moment of transient heating, the samples do not have time to expand and are thus in a compression state. To release the stresses, the lattice expansion starts from free surfaces to the insides, appearing as the propagation of acoustic waves carrying the tendency of tensile elastic strains. At the early stage, the inner regions are still undisturbed, as shown on the section planes of the NPG model [Fig. 3(a)] and the PCG model [Fig. S5(a)]. The stresses in the inner regions of the NPG ligaments and the PCG film are still compressive, while the stresses in the regions around the free surfaces have been partly released. The tensile acoustic waves keep propagating and make the stress-released areas over-expanded until they are reflected from the opposite surfaces and start to carry the tendency of contraction. Therefore, when the averaged expansion reaches the maximum, most inner regions of the samples are stretched [Figs. (3b) and S5(b)]. At this moment, the plane wave fronts in the PCG film just reach the opposite surfaces and start to travel backward. On the contrary, the surface-launched acoustic waves are divergent and out of sync in NPG due to the variation of NPG ligament shapes and sizes, and thus reach the opposite surfaces in different directions at different paces. As a result, the stress distribution around the free surfaces of the NPG ligaments appears random (Fig. S6), and the stretched regions and the compressed regions are interspersed around the free surfaces. Following the expansion, the samples start to contract when most of the acoustic waves are reflected. As the reflected waves in the NPG ligaments become more divergent and more out of sync, the stress distribution becomes more diverse during the contraction. Some regions in large-size ligaments are still stretched, and some in small-size ligaments are already stress-released or compressed again [Fig. 3(c)] even when the averaged contraction reach the maximum [Fig. 3(d)]. In contrast, the contraction of materials in the PCG film is almost the reverse process of the previous expansion with slight acoustic damping [Figs. S5(c) and S5(d)]. The GHz acoustic waves keep propagating and reflecting during the expansion–contraction cycles by the repeating conversion between elastic energy and kinetic energy. The energy relaxation process takes place in the energy conversion during the propagation of acoustic waves by acoustic energy dissipation. As we compared the stress distribution in the second cycle to that

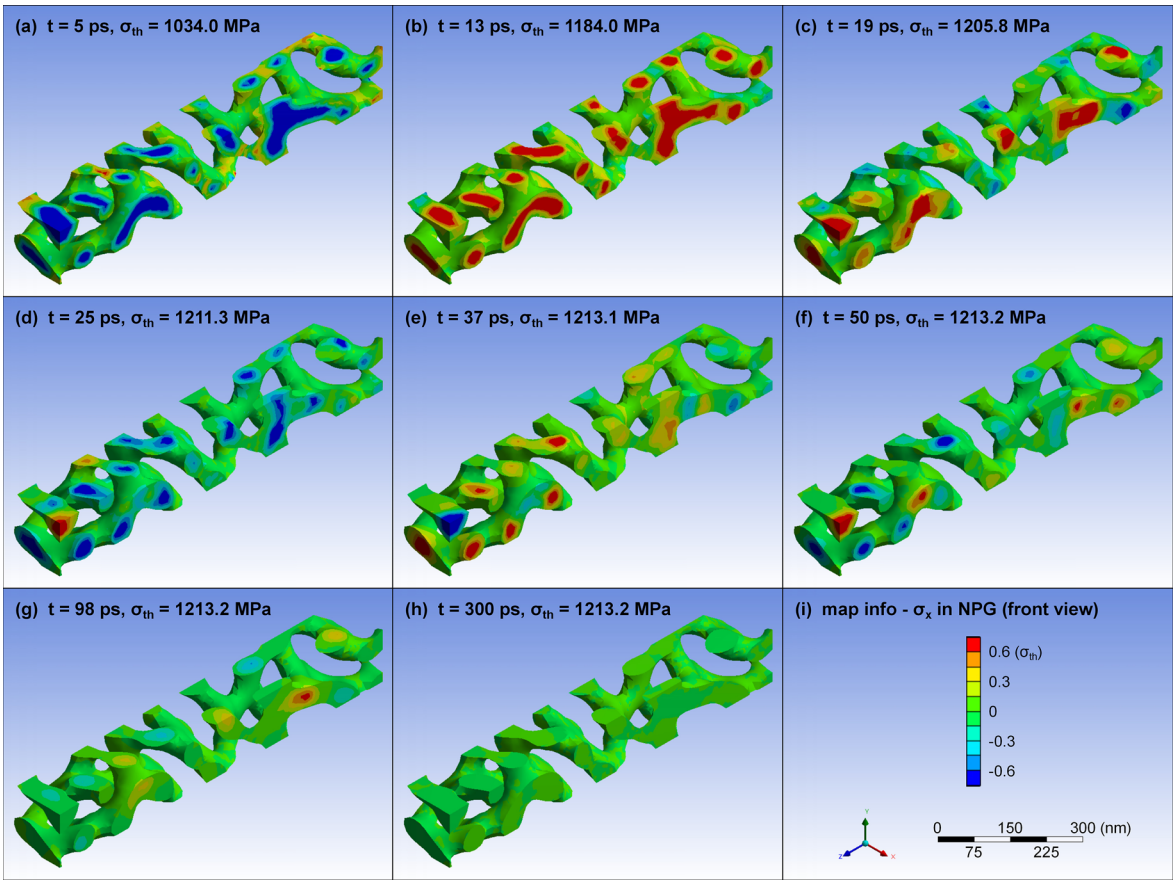

FIG. 3. The stress distribution on the cross sections of NPG at different time delays.

in the first cycle for both NPG and PCG, the overall stretch or compression stresses become obviously less at the maxima of the averaged expansion [Figs. 3(e) and S5(e)] or contraction [Figs. 3(f) and S5(f)], suggesting the gradual dissipation of the acoustic energy during the oscillation in both samples. As mentioned above, the energy of the experiment samples in the detected areas has not been dissipated into the undetected areas or the environment in the timescale of our experiments. Therefore, the samples can be considered as adiabatic systems in the FEM calculations, and thus all of the dissipated acoustic energy is converted into heat and then is ignored during the simulations.

We quantified the temporal evolution of the remained acoustic energy density relative to the total acoustic energy density E_a/E in both systems. The total acoustic energy density in the system is

$$E(t) = \frac{\sigma^2(t)}{2K}, \tag{5}$$

and the remained acoustic energy density can be expressed as

$$E_a(t) = E_p(t) + E_k(t) = \frac{1}{V}\int\int\int_V \sum_{i,j}\frac{\sigma_{ij}\varepsilon_{ij}}{2} + \sum_i \frac{\rho {v_i}^2}{2}\mathrm{d}V, \tag{6}$$

where E_p and E_k refer to the remained elastic and kinetic energy density; σ_{ij}, ε_{ij}, and v_i refer to the stress, strain, and velocity components in Cartesian coordinates as functions of position and time; ρ is the mass density; V is the total volume; and $\int\int\int_V \mathrm{d}V$ means the overall spatial integration. It is confirmed that the portion of dissipated acoustic energy increases with the wave propagation [Fig. 4(a)] during the repeating conversion between elastic [Fig. S7(a)] and kinetic energies [Fig. S7(b)]. Note that the portion of dissipated acoustic energy $(1 - E_a/E)$ in the NPG system is significantly larger than that in PCG with a ratio of >121% between the two systems. In our calculations, the in-plane squeeze of the samples does not exceed the in-plane constrained borders. For the PCG system, the confinement makes only out-of-plane straining allowed, leading to a one-dimensional expansion and thus a steady-state volume change of $\alpha\Delta T_{l,\infty}(1+\nu)/(1-\nu)$, where ν is the Poisson's ratio and is 0.425 for gold.[28] In contrast, due to the existence of nanopores in NPG, the outer confinement cannot prevent the in-plane expansion of individual ligaments and thus the expansion is three-dimensional with the steady-state volume change of $3\alpha\Delta T_{l,\infty}$. The different volume changes make the expansion energy partly stored in PCG as the elastic energy but fully released in NPG in the form of acoustic waves. The stored elastic energy in PCG can be released only after the in-plane constraint is removed, i.e., the acoustic waves propagate from the homogeneously pumped area border to the probed area border, which takes about tens of nanoseconds, much larger than the timescale we investigated.

The energy dissipation of the acoustic waves with the generation of heat essentially leads to the break of collective motion of atoms by

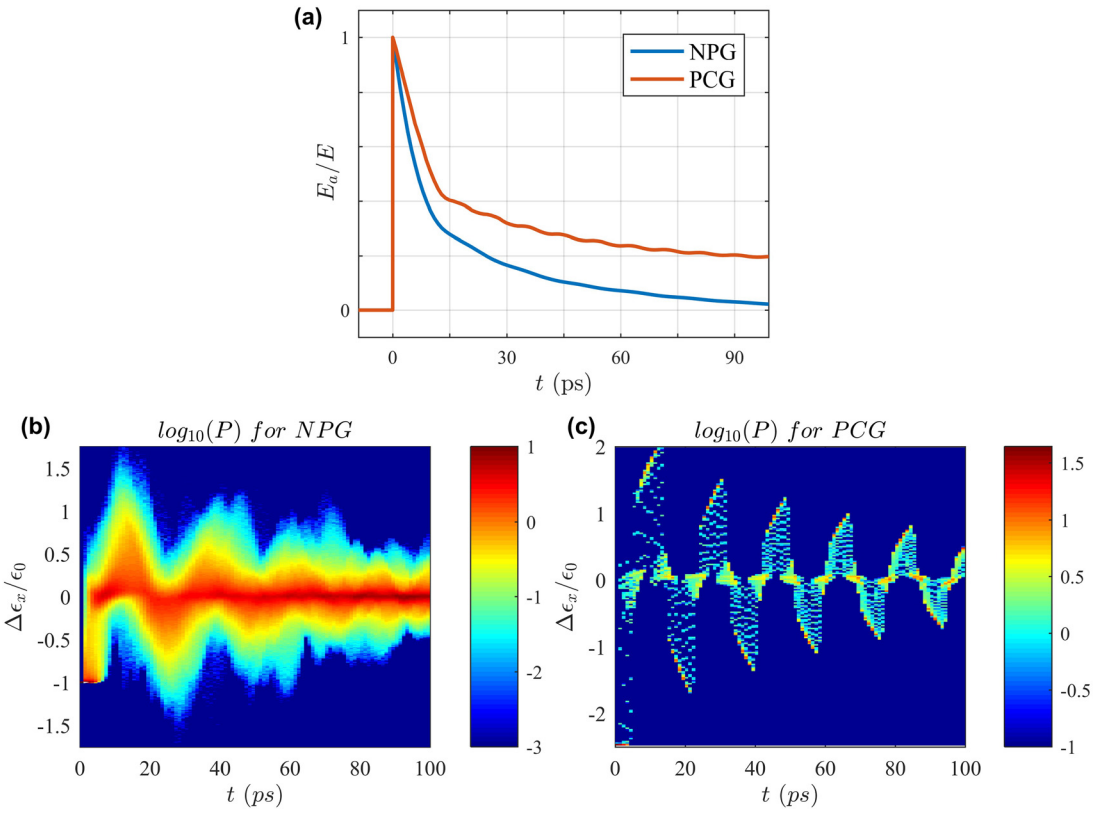

FIG. 4. (a) The evolution of the remained acoustic energy density relative to the total acoustic energy density E_a/E for NPG and PCG. (b) and (c) The logarithm of strain distribution probability $\log_{10}(P)$ for NPG and PCG, where $\varepsilon_0(t)$ is the steady linear strain with thermal stress $\sigma(t)$. Note that $\int P\mathrm{d}(\varepsilon_x/\varepsilon_0) = 1$.

introducing random atomic displacements. In the FEM calculations, the existing atomic random vibration and the enhancement due to damping have been ignored, while the atomic motion away from the local equilibrium position during lattice expansion is considered as local strain. As a result, the strain distribution in NPG appears "random" [Fig. 4(b)], unlike the "tidy" strain distribution in PCG [Fig. 4(c)]. In consequence of the staggered reflection in NPG ligaments with different sizes, the convergence or divergence by irregular ligaments, and the propagation in the tortuous ligaments with different orientations, the launched acoustic waves become divergent and out of sync during propagation. Therefore, the strain distribution in NPG becomes dispersive right after the uniform initial straining and then gradually converges toward the oscillating average value, along with the fast oscillation decaying. It corresponds to the atomic motion from sync to random during the lattice expansion. In the frequency domain it indicates the acoustic phonons with low coherence excited in NPG, distinct from the coherent acoustic phonons in PCG.

For better understanding the dynamic behavior of the GHz acoustic waves in NPG, we utilized the concept of driven damped harmonic oscillators[11] and developed a general description in frequency domain (see Derivation in supplementary material). The acoustic waves can be decomposed into the superposition of a set of eigenmodes which represent the driven damped harmonic oscillators. The displacement of n th eigenmode $\boldsymbol{u}_n(\boldsymbol{r}, t)$ can be expressed as

$$\boldsymbol{u}_n(\boldsymbol{r}, t) = [G_n(t) + P_n(t)]\boldsymbol{U}_n(\boldsymbol{r}), \tag{7}$$

where $\boldsymbol{U}_n(\boldsymbol{r})$ is the normalized displacement field, and $G_n(t)$ and $P_n(t)$ are the time-dependent amplitudes of general damped part and particular steady state, representing the damped acoustic phonon and its oscillation center shift. The morphology of the laser excited objects determines the allowed $\boldsymbol{U}_n(\boldsymbol{r})$ and corresponding undamped angular frequency ω_n, which are subjected to the governing equation and the stress-free boundary condition. For high symmetric objects, such as in-plane-constraint plate, axial-constraint cylinder, and sphere, it gives

$$\omega_n = k_n v_L \tag{8}$$

and the required results when $n = 2m - 1$ or $n = 2m$,

$$\left\{ \begin{array}{l} U_{2m-1}(r) = \dfrac{\sin(k_{2m-1}r)}{\sin(k_{2m-1}R)},\ U_{2m}(r) = \dfrac{\cos(k_{2m}r)}{\cos(k_{2m}R)} \\ U_{2m-1}(r) = \dfrac{J_1(k_{2m-1}r)}{J_1(k_{2m-1}R)},\ U_{2m}(r) = \dfrac{Y_1(k_{2m}r)}{Y_1(k_{2m}R)} \\ U_{2m-1}(r) = \dfrac{j_1(k_{2m-1}r)}{j_1(k_{2m-1}R)},\ U_{2m}(r) = \dfrac{y_1(k_{2m}r)}{y_1(k_{2m}R)} \end{array} \right\}, \tag{9}$$

where m is an integer; r is the distance from plate center plane, cylinder centerline, or sphere center point in Cartesian, cylindrical, or spherical coordinate; R is the characteristic size of object, which is half thickness for plate, radius for cylinder, or radius for sphere; J_x, Y_x and

j_x, y_x are the Bessel functions and spherical Bessel functions of x order; and k_n are the morphology-related wave vectors,

$$\left\{\begin{array}{c} k_n = \dfrac{n\pi}{2R} \\ k_n \approx \dfrac{n\pi}{2R} + \dfrac{\pi}{4R} \\ k_n \approx \dfrac{n\pi}{2R} + \dfrac{\pi}{2R} \end{array}\right\}. \tag{10}$$

Due to the structure difference between NPG and PCG, $\boldsymbol{U}_n(\boldsymbol{r})$ and corresponding ω_n of excited acoustic phonons are distinct. In the solid PCG film with a well-defined thickness, the out-of-plane acoustic waves can be decomposed into the superposition of one-dimensional coherent acoustic phonons with discrete frequencies. In contrast, the lack of nanoscale structural periodicity in NPG allows more three-dimensional acoustic phonon modes with a wide range of frequencies. Therefore, the initially excited acoustic phonons with low coherence in NPG correspond to a distribution of phonons, which is close to the thermal distribution of dispersive phonon modes. The low coherence refers to the gradual loss of synchronization of random atomic motion in time domain, i.e., limited coherence time of acoustic phonons due to a wide range of frequencies,[19] which leads to random atomic motion. Thus, the increased damping of observed peak position oscillations in NPG is predominantly due to dephasing of excited phonons and not due to an increased inelastic damping which is described by the Rayleigh damping factors in the FEM calculations. However, the ignored phonons generated from the inelastic damping of initially excited phonons, represented by the damping of $G_n(t)$, are consequently more dispersive, accelerating the establishment of thermal state. Therefore, the complex nanoporous structure of NPG promotes dispersive phonon states and the establishment of equilibrium phonons, namely, accelerates the dissipation of lattice expansion energy to heat. The excitation of acoustic phonons is also morphologically dominated, so the morphological inhomogeneity of the nanoporous structures of NPG also plays an important role in accelerating the energy dissipation of GHz–THz acoustic waves, in addition to the known diffraction, thermo-elastic damping, grain boundary scattering, so on. In fact, the significant effect of bicontinuous nanoporosity on the high-frequency elastic wave attenuation suggests that dealloyed nanoporous metals with tunable pore sizes[30] could be ideal materials as GHz and THz acoustic filters and dampers.

In summary, we have studied the high-frequency acoustic responses of free-standing NPG and PCG films by the MeV UED technique and FEM simulations. By tracing the evolution of acoustic waves in time domain and describing the acoustic phonons in frequency domain, we found that the bicontinuous nanoporous structure in dealloyed NPG films leads to three-dimensional and acoustic response with low coherence, resulting in the full release and rapid attenuation of GHz–THz acoustic waves by fast energy dissipation. The nanostructure dominated acoustic phonon dynamics demonstrates that 3D bicontinuous nanoporosity plays an important role in the attenuation of high frequency elastic waves and shines a light on the applications of dealloyed nanoporous metals as GHz and THz acoustic filters and dampers in nanodevices and nanosensors.

See the supplementary material for figures and derivation of equations (PDF).

This work was supported by the National Science Foundation (No. NSF DMR-1804320), the U.S. Department of Energy Contract No. DEAC02-76SF00515, the SLAC UED/UEM Initiative Program Development Fund, JST-CREST Phase Interface Science for Highly Efficient Energy Utilization, Japan Science and Technology Agency, and the Deutsche Forschungsgemeinschaft (DFG, German Research Foundation) through the Collaborative Research Centre (CRC) 1242 (Project No. 278162697, project C01 Structural Dynamics in Impulsively Excited Nanostructures).

DATA AVAILABILITY

The data that support the findings of this study are available within the article and its supplementary material.

REFERENCES

[1]H. J. Mamin and D. Rugar, Appl. Phys. Lett. **79**, 3358 (2001).
[2]J. Chaste, A. Eichler, J. Moser *et al.*, Nat. Nanotechnol. **7**, 301 (2012).
[3]K. Jensen, K. Kim, and A. Zettl, Nat. Nanotechnol. **3**, 533 (2008).
[4]C. Thomsen, H. T. Grahn, H. J. Maris, and J. Tauc, Phys. Rev. B **34**, 4129 (1986).
[5]C. Thomsen, J. Strait, Z. Vardeny *et al.*, Phys. Rev. Lett. **53**, 989 (1984).
[6]M. Hu, X. Wang, G. V. Hartland *et al.*, J. Am. Chem. Soc. **125**, 14925 (2003).
[7]P. Zijlstra, A. L. Tchebotareva, J. W. M. Chon, M. Gu, and M. Orrit, Nano Lett. **8**, 3493 (2008).
[8]P. V. Ruijgrok, P. Zijlstra, A. L. Tchebotareva, and M. Orrit, Nano Lett. **12**, 1063 (2012).
[9]M. Nisoli, S. De Silvestri, A. Cavalleri *et al.*, Phys. Rev. B **55**, R13424 (1997).
[10]G. V. Hartland, Annu. Rev. Phys. Chem. **57**, 403 (2006).
[11]A. Crut, P. Maioli, N. D. Fatti, and F. Vallée, Phys. Rep. **549**, 1 (2015).
[12]M. Nicoul, U. Shymanovich, A. Tarasevitch, D. von der Linde, and K. Sokolowski-Tinten, Appl. Phys. Lett. **98**, 191902 (2011).
[13]S. Nie, X. Wang, H. Park, R. Clinite, and J. Cao, Phys. Rev. Lett. **96**, 025901 (2006).
[14]X. Wang, S. Nie, J. Li *et al.*, Appl. Phys. Lett. **92**, 121918 (2008).
[15]T. Henighan, M. Trigo, S. Bonetti *et al.*, Phys. Rev. B **93**, 220301 (2016).
[16]A. E. H. Love, *A Treatise on the Mathematical Theory of Elasticity* (Cambridge University Press, 1892).
[17]C. Prada, O. Balogun, and T. W. Murray, Appl. Phys. Lett. **87**, 194109 (2005).
[18]L. L. Beranek, J. Acoust. Soc. Am. **13**, 248 (1942).
[19]N. Lopez-Abdala, M. Esmann, M. C. Fuertes *et al.*, J. Phys. Chem. C **124**, 17165 (2020).
[20]T. Fujita, L. H. Qian, K. Inoke, J. Erlebacher, and M. W. Chen, Appl. Phys. Lett. **92**, 251902 (2008).
[21]S. P. Weathersby, G. Brown, M. Centurion *et al.*, Rev. Sci. Instrum. **86**, 073702 (2015).
[22]Q. Zheng, X. Shen, K. Sokolowski-Tinten *et al.*, J. Phys. Chem. C **122**, 16368 (2018).
[23]J. Hohlfeld, S.-S. Wellershoff, J. Güdde *et al.*, Chem. Phys. **251**, 237 (2000).
[24]B. O. Wright, Phys. Rev. B **49**, 9985 (1994).
[25]S. Nie, X. Wang, J. Li, R. Clinite, and J. Cao, Microsc. Res. Tech. **72**, 131 (2009).
[26]K. Sokolowski-Tinten, X. Shen, Q. Zheng *et al.*, Struct. Dyn. **4**, 054501 (2017).
[27]K. O. Mclean, C. A. Swenson, and C. R. Case, J. Low Temp. Phys. **7**, 77 (1972).
[28]K. A. Gschneidner, Jr., Solid State Phys. **16**, 275 (1964).
[29]A. Cavalleri, C. W. Siders, F. L. H. Brown *et al.*, Phys. Rev. Lett. **85**, 586 (2000).
[30]L. Qian and M. Chen, Appl. Phys. Lett. **91**, 083105 (2007).